Article

Cell Reports

Intratumoral Cancer Cell Intravasation Can Occur Independent of Invasion into the Adjacent Stroma

Graphical Abstract

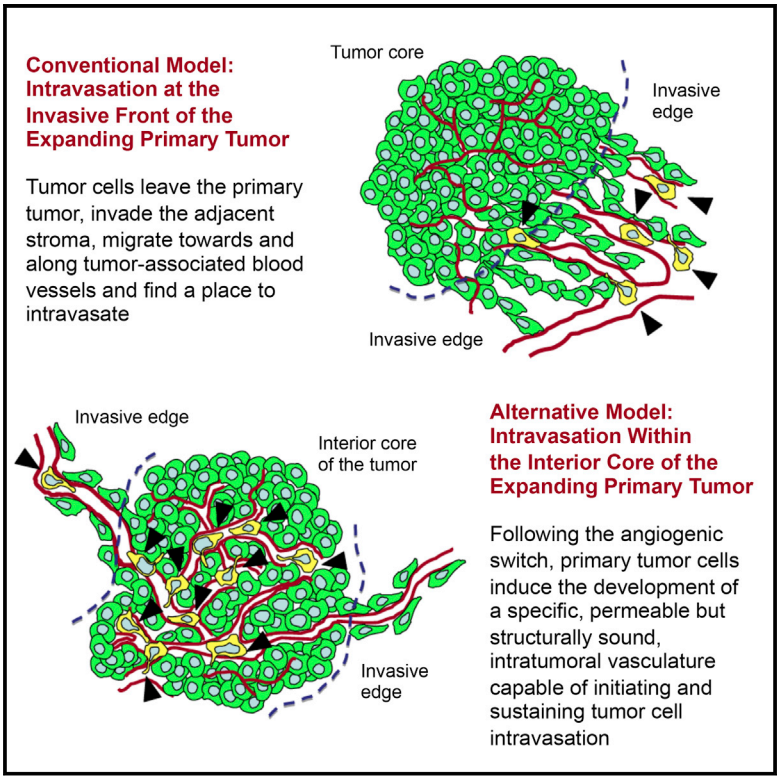

Highlights

- Intravasation can be initiated early on and proceed in parallel to stromal invasion
- Intravasation occurs almost exclusively in the interior core of the primary tumor
- Intravasation is insignificant within the invasive outgrowths along blood vessels
- EGFR is required for developing an intravasation-sustaining vasculature

Authors

Elena I. Deryugina, William B. Kiosses

Correspondence

deryugin@scripps.edu

In Brief

Deryugina and Kiosses investigate the localization of intravasation within primary tumors. They find that the majority of intravasation events occur within the tumor core and not at the invasive edge within tumor outgrowths into adjacent stroma in the models examined. Mechanistically, EGFR appears to impact intratumoral intravasation by regulating development of a fully interconnected angiogenic vasculature.

Deryugina & Kiosses, 2017, Cell Reports *19*, 601–616
April 18, 2017
http://dx.doi.org/10.1016/j.celrep.2017.03.064

CellPress

Cell Reports
Article

Intratumoral Cancer Cell Intravasation Can Occur Independent of Invasion into the Adjacent Stroma

Elena I. Deryugina[1,3,*] and William B. Kiosses[2]
[1]Department of Molecular Medicine
[2]Confocal Microscopy Core Facility
The Scripps Research Institute, 10550 North Torrey Pines Road, La Jolla, CA 92037, USA
[3]Lead Contact
*Correspondence: deryugin@scripps.edu
http://dx.doi.org/10.1016/j.celrep.2017.03.064

SUMMARY

Intravasation, active entry of cancer cells into the circulation, is often considered to be a relatively late event in tumor development occurring after stromal invasion. Here, we provide evidence that intravasation can be initiated early during tumor development and proceed in parallel to or independent of tumor invasion into surrounding stroma. By applying direct and unbiased intravasation-scoring methods to two histologically distinct human cancer types in live-animal models, we demonstrate that intravasation takes place almost exclusively within the tumor core, involves intratumoral vasculature, and does not involve vasculotropic cancer cells invading tumor-adjacent stroma and migrating along tumor-converging blood vessels. Highlighting an additional role for EGFR in cancer, we find that EGFR is required for the development of an intravasation-sustaining intratumoral vasculature. Intratumoral localization of intravasation supports the notion that overt metastases in cancer patients could be initiated much earlier during cancer progression than appreciated within conventional clinical tumor staging systems.

INTRODUCTION

Metastasis, the leading cause of cancer-related deaths, is a multi-staged process that includes as a critical step an intravasation event involving active entry of cancer cells into the vasculature. Intravasation is often regarded as a relatively late process during cancer progression, initiated after aggressive cancer cells undergo epithelial-mesenchymal transition (EMT), breach the epithelial basement membrane, invade the surrounding stroma, and reach tumor-coalescing blood vessels, which the escaped cells then penetrate to enter the circulation. This widely accepted sequence of ''linear cascade'' processes, ultimately culminating in the metastatic colonization of distal organs via hematogenous routes, is supported by experimental and clinical data consistently indicating that cancer metastasis is associated with local invasion beyond the original primary tumor boundaries and tumor angiogenesis providing vascular conduits for disseminating tumor cells (Hanahan and Weinberg, 2011; Weinberg, 2013).

The linear cascade model, however, is at odds with accumulating evidence suggesting that the onset of cancer metastasis occurs much earlier in tumor development than is generally indicated by conventional clinical staging of primary tumors during cancer patient diagnosis (Massagué and Obenauf, 2016; Turajlic and Swanton, 2016). According to retrospective clinical data, the establishment of clinically relevant metastases can take place at stages *preceding* substantial local invasion by primary tumors (Cochet et al., 2014; Fibla et al., 2013; Riedl et al., 2014; Suh et al., 2013; Yoshida et al., 2013). The concept of early metastases is also supported by mathematical computation of the time required for distant outgrowths to become life-threatening metastases (Coumans et al., 2013; Hölzel et al., 2010). Murine models also support an early onset of metastasis by demonstrating that distant micrometastases can be established from benign tumors (Hüsemann et al., 2008) or even by untransformed cells (Podsypanina et al., 2008), acquiring malignancy at the secondary site independent of primary tumor progression (Klein, 2009). In a mouse model of pancreatic cancer, metastasis-seeding cells were detected in the bloodstream before frank malignancy was detected histologically (Rhim et al., 2012), suggesting that primary tumor cells entered the circulation ahead of initiation of stromal invasion. Importantly, both clinical and experimental studies have provided strong evidence that the angiogenic switch, a prerequisite for intravasation and metastasis, is triggered during the early, pre-invasive stage of tumor development (Folkman, 2002).

Intravasation is a complex in vivo process that cannot be fully modeled in vitro and is rarely observed in vivo (Wyckoff et al., 2007). Therefore, intravasation levels are determined by indirect methods such as quantifying vascular-arrested tumor cells in distal tissues (Kim et al., 1998) or circulating tumor cells in the peripheral blood (Wyckoff et al., 2007). Intravital imaging of primary tumors in tumor-bearing animals does offer insights into the process of tumor cell intravasation (Chiang et al., 2016) but does not provide the capacity to quantify intravasation events across entire primary tumors and in multiple animals. Because of these methodological limitations, the spatiotemporal localization of actual intravasation events has never been investigated, and the topography of intravasation process remains unknown.

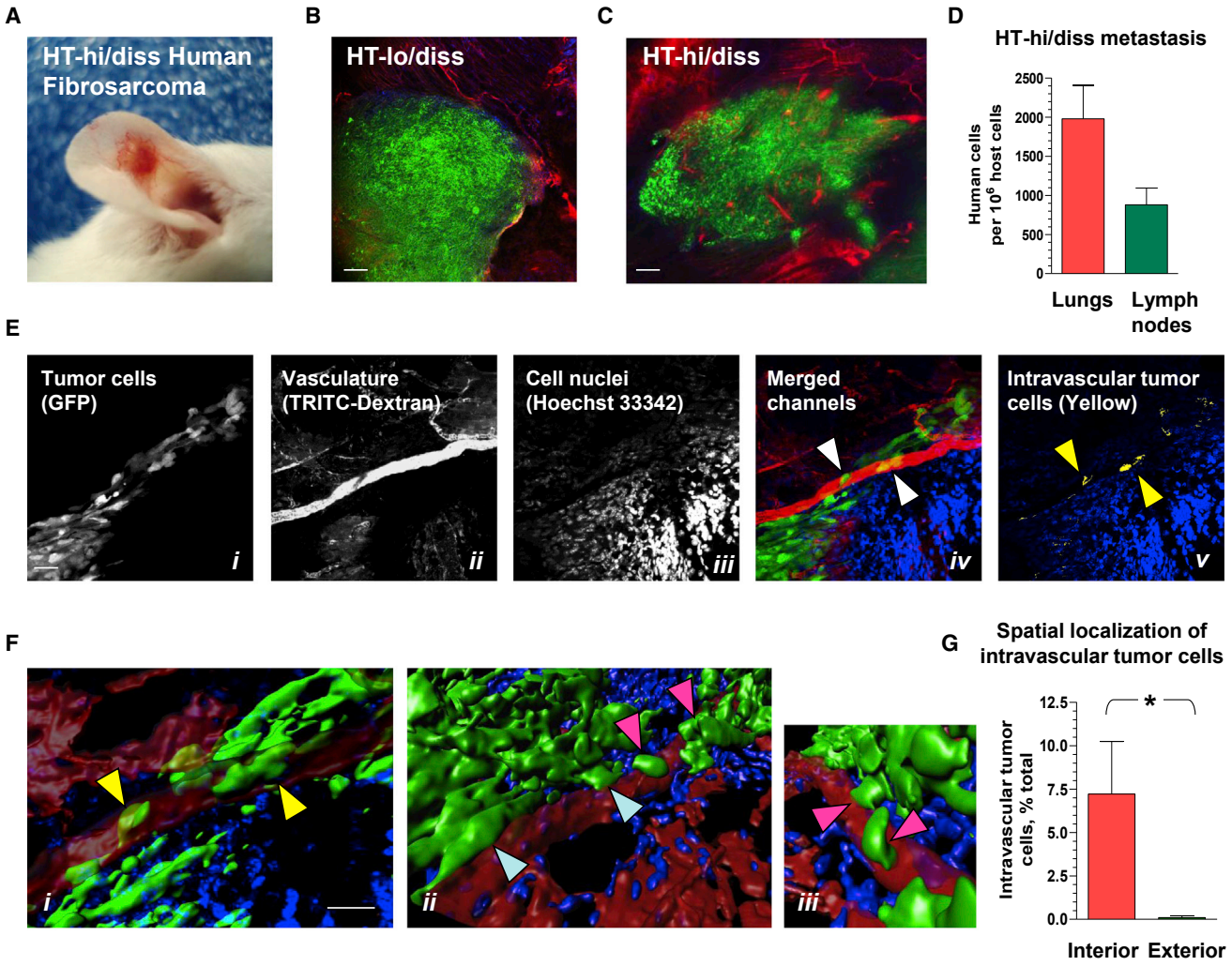

(legend on next page)

To study the mechanisms of intravasation, we have established model systems for molecular probing and quantification of angiogenesis-dependent intravasation in live animals (Deryugina and Quigley, 2008; Deryugina et al., 2014). Human tumor congenic variants were selected for high and low intravasation ability and, correspondingly, high and low levels of intravasation-dependent metastasis (Conn et al., 2009; Deryugina et al., 2005; Juncker-Jensen et al., 2013). In the present study, fully automated intravasation-scoring methods were developed to directly visualize and count intravasation events based on an unbiased determination of the intraluminal versus abluminal position of all cancer cells constituting the developing tumor. Thus, it is possible to delineate and quantify a distinct population of intravascularly located tumor cells and localize actual intravasation events within the entire primary tumor, including its interior core and invasive outgrowths along tumor-converging blood vessels.

Herein, spatial localization of intravasation was investigated in invasive tumors generated by highly disseminating cancer cells of distinct histological origin (fibrosarcoma and carcinoma), employed in two animal models, a chick embryo model (Deryugina and Quigley, 2008) and a mouse model (Bobek et al., 2010). Unexpectedly, spatial analysis of intravasation in distinct areas of primary tumors indicated that the vast majority (>90%) of intravasation events were localized not to stroma-invading outgrowths, but to the interior angiogenic core. We also demonstrate that the tumor cell EGFR is required for the development of an intravasation-sustaining intratumoral vasculature. Together, our findings suggest that a metastasis-seeding intravasation process can be initiated early on in developing primary tumors and proceed within the interior core independent of ensuing stromal invasion.

RESULTS

Topography of Cancer Cell Intravasation in the Mouse Ear Model System

Monitoring and visualization of tumor cell intravasation events in a mammalian setting was conducted in a mouse ear that provides dense vascular bed in the dermis and relatively thin stromal tissue. The feasibility was verified in a syngeneic model by employing aggressive murine B16-F10 melanoma cells in C57BL/6 mice (Figure S1). We adopted this model to a xenogeneic setting by implanting human fibrosarcoma cell variants (low metastatic HT-lo/diss and high metastatic HT-hi/diss) into immunodeficient NOD-SCID mice (Figure 1A). Two weeks after implantation of GFP-tagged cells, the vasculature in tumor-bearing mice was highlighted in vivo with tetramethylrhodamine (TRITC)-dextran. Epifluorescent microscopy demonstrated that HT-lo/diss tumors were largely confined, displaying a smooth border and low levels of intratumoral vascularization (Figure 1B). In contrast, HT-hi/diss tumors appeared highly invasive with extensive neovascularization within and around tumor border (Figure 1C). Two weeks after primary tumor removal, HT-hi/diss cells were identified by *Alu*-qPCR in the lungs and inguinal lymph nodes (Figure 1D), indicating model suitability for investigating metastatic dissemination of human tumor cells. Furthermore, no human cells above the background levels were detected in the lymph nodes and lungs by highly sensitive human-specific *Alu*-qPCR immediately after tumor cell grafting, supporting a view that lung metastases originated from cells that disseminated from developing primary tumors.

Segments of whole-mounted HT-hi/diss tumors were imaged with a confocal microscope (Figures 1Ei–iii), and merged-channel images indicated intravascular tumor cells (Figure 1Eiv). Using Imaris, these tumor cells were assigned a separate signal (Figure 1Ev), and their intravascular position was confirmed by comparison of translucent versus opaque modes of Imaris-rendered 3D images (Figure 1F, i versus ii). The opaque mode enabled us to clearly visualize the tumor cells positioned extravascularly at the abluminal surface of the blood vessel (Figure 1Fii), while a rotation of the 3D-reconstructed images allowed us to visualize tumor cells that appear as entering the vessel lumen (Figure 1F, ii versus iii). Automated quantification across individual slices of HT-hi/diss tumors demonstrated that intravascular tumor cells identified within the primary tumor core constituted 7.2% ± 3.7% of total tumor cells within the slice. Strikingly, only 0.1% ± 0.1% of tumor cells were intravascularly positioned within the stroma-invading outgrowths (Figure 1G), indicating that the vast majority (>98%) of intravasated cells were localized to the core of primary tumors.

Figure 1. Cancer Cell Intravasation in the Mouse Ear Model System

(A) Highly vascularized HT-hi/diss primary tumor developing in the ear of NOD-SCID mice.

(B and C) HT-lo/diss (B) and HT-hi/diss (C) primary tumors examined by immunofluorescent microscopy: green, GFP-tagged tumor cells; red, vasculature highlighted with i.v.-inoculated TRITC-dextran. Bars, 250 μm.

(D) HT-hi/diss metastasis in the lungs (n = 4) and lymph nodes (n = 8) quantified by human *Alu*-qPCR. Data are shown as mean ± SEM.

(E) HT-hi/diss primary tumor examined by scanning laser confocal microscopy: GFP-tagged tumor cells (i), dextran-highlighted vasculature (ii), and cell nuclei highlighted by NucBlue (iii); the merged-channel image (iv) depicts tumor cells in green, vasculature in red, and cell nuclei in blue. Imaris software was employed to identify intravascularly located tumor cells (v, yellow signal and arrowheads). Bar, 25 μm.

(F) High-resolution analysis of tumor cells located intravascularly (i, yellow arrowheads), abluminal along vessel surface (ii, blue arrowheads), or appearing as entering into the vessel (iii, pink arrowheads). Bar, 25 μm.

(G) Automated quantification of intravascular tumor cells localized either to the inner portion of primary tumors (interior) or to stroma-invading outgrowths (exterior). A total of 540 cells were identified as intravascular cells, among which 532 cells (98.5%) were localized to the center of primary tumors (n = 4). Data are shown as mean ± SEM. *$p < 0.05$.

(H) Schematic models depicting spatial localization of intravasation process. Left, according to a *conventional* model, intravasation occurs beyond original tumor boundaries, and, therefore, intravasation events (yellow) would mainly be localized at the invasive front within tumor-converging blood vessels, co-opted, or newly formed. Right, according to an *alternative* model, supported by the findings of this study, the intravasation process occurs almost exclusively within the core of the primary tumor, and, therefore, intravasation events (yellow) are localized to the intratumoral angiogenic vasculature.

Thus, our scoring assay is well suited for investigation of the actual topographical position of intravasated tumor cells across an entire primary tumor. According to a conventional model (Figure 1H, left), the majority of intravasation events are expected to be within tumor-coalescing blood vessels (co-opted or newly formed during the invasive stage), at or beyond the primary tumor boundaries Alternatively, the bulk of intravasation events could be localized to angiogenic blood vessels in the interior core of a primary tumor (Figure 1H, right), and therefore the intravasation process would early on be uncoupled from the formation of the leading edge and invasion of adjacent stroma, as defined in clinical staging. Since the relatively large size of ear tumors and therefore the large amount of time necessary for image acquisition makes it difficult to conduct systematic analyses of tumor cell localization within entire primary tumors in multiple animals, we employed a more feasible method for resolving the precise topography of the intravasation process.

Avian Model System for Quantitative Analysis of Cancer Cell Intravasation

To spatially localize and quantify actual intravasation events within whole primary tumors, we employed a microtumor assay in which GFP-tagged human tumor cells were inoculated into the chorioallantoic membrane (CAM) mesoderm of chick embryos. Within 5 days after implantation, both HT-lo/diss and HT-hi/diss cells formed intramesodermal tumors; however, only hi/diss tumors exhibited extensive invasion into adjacent stroma (Figure 2A). Furthermore, escaping HT-hi/diss cells demonstrated significant vasculotropism manifested in their stromal invasion along tumor-adjacent blood vessels in close association with the abluminal surface of blood vessels (Figure 2B). On average, vasculotropic HT-hi/diss cells invaded the stroma at distances reaching 500 μm from the tumor core border and exceeding 10-fold distances traveled by HT-lo/diss cells (Figure 2C). Detailed analyses also demonstrated that, while more than 25% of all escaping HT-hi/diss cells were intimately associated with blood vessels, less than 3% of HT-lo/diss cells exhibited such vasculotropic behavior (Figure 2D). This differential in vasculotropism was confirmed in our ex vivo 3D model designed to quantify tumor cell migration toward excised blood vessels (Figure 2E). In this model, approximately ten times more HT-hi/diss cells migrated through 3D collagen in response to CAM vessels compared to HT-lo/diss cells (Figure 2F), thereby validating the high vasculotropism of invasive HT-hi/diss cells in vivo (Figure 2D). Since both primary tumor cores and invasive outgrowths are formed in the intramesodermal HT-hi/diss tumors, this model appeared ideal to study spatial localization of the intravasation process.

Discrimination between Intraluminal and Abluminal Positioning of Cancer Cells within the Primary Tumor

The approach is based on multiparameter analysis of entire primary tumors for which individual scanned regions were multi-stitched in 3D using Zen software. Confocal microscopy was conducted on intramesodermal tumors initiated from GFP-tagged HT-lo/diss or HT-hi/diss cells. Tumor vasculature was stained in vivo with red fluorescent lectin. The stitched 20× z stacks confirmed the largely non-invasive nature of HT-lo/diss tumors (Figure 3A, top left). In contrast, HT-hi/diss tumors developed both a primary core and multiple stromal outgrowths along tumor-converging blood vessels (Figure 3B, top). This difference in the invasive abilities of two dissemination variants suggested that HT-hi/diss cells might intravasate outside the tumor border at the invasive front, in agreement with conventional cancer progression models. However, since spatial topography of the intravasation process throughout an entire primary tumor has never been quantified, we sought to address this issue in a quantitative and unbiased manner employing our newly developed models and specifically tailored microscopy approaches.

High-resolution images of selected areas in HT-hi/diss tumors (the boxed area in Figure 3B) were captured at 40× and rendered three-dimensional with Imaris module (Figure 3C). The translucent mode (Figure 3C, top) allowed us to distinguish intravascularly located tumor cells, which become invisible when the vessel surface is made opaque (Figure 3C, bottom). Furthermore, at the level of a single primary tumor slice imaged with high resolution at 63× (Figure 3D, left), individual tumor cells can be clearly discriminated either as entering the blood vessels or located at the abluminal surface of the vessels (Figure 3D, i and ii). By applying the Imaris colocalization module with a conservative threshold, the signal for tumor cells that were localized entirely in the vessels or crossing the vessel wall was delineated and rendered a new color (yellow in Figures 3A and 3B, bottom). This signal was significantly lower in HT-lo/diss tumors compared to HT-hi/diss tumors (Figure 3E), even though both tumor types had similar levels of vascularization (Figure 3F). Surprisingly, the signal for intravascular/intravasating HT-hi/diss cells was associated mainly with the inner portion of primary tumors and much less with the stromal outgrowths along tumor-converging blood vessels (Figure 3B, top versus bottom). Therefore, this model provided a unique approach for developing a method for unbiased identification and quantification of actual intravasation events in different areas of the primary tumor.

Localization and Quantification of Intravasation Events within the Entire Primary Tumor

HT-hi/diss tumors develop a dense network of angiogenic blood vessels within the primary tumor core and also induce a network of blood vessels, converging on the primary tumor border and serving as tracks for escaping tumor cells (Figure 4A). We designed a unique image analysis allowing for a software-assisted quantification of actual intravasation events throughout the entire area occupied by primary tumor cells (Figure 4B). Using MATLAB macros within the Imaris software and isosurfacing modules, a scoring method was developed to determine unambiguously whether or not a tumor cell is localized completely within the vessel lumen (Figure S2). This method involves the thresholding of the original vascular signal and creating a 3D-rendered tubular isosurface. This process is performed twice, first to outline vessel tubes and then to fill in the tubular structures to render them solid. A distance transform module is used to define in color (a violet-to-red scale) the distances at which each and all tumor cells are located from the center of

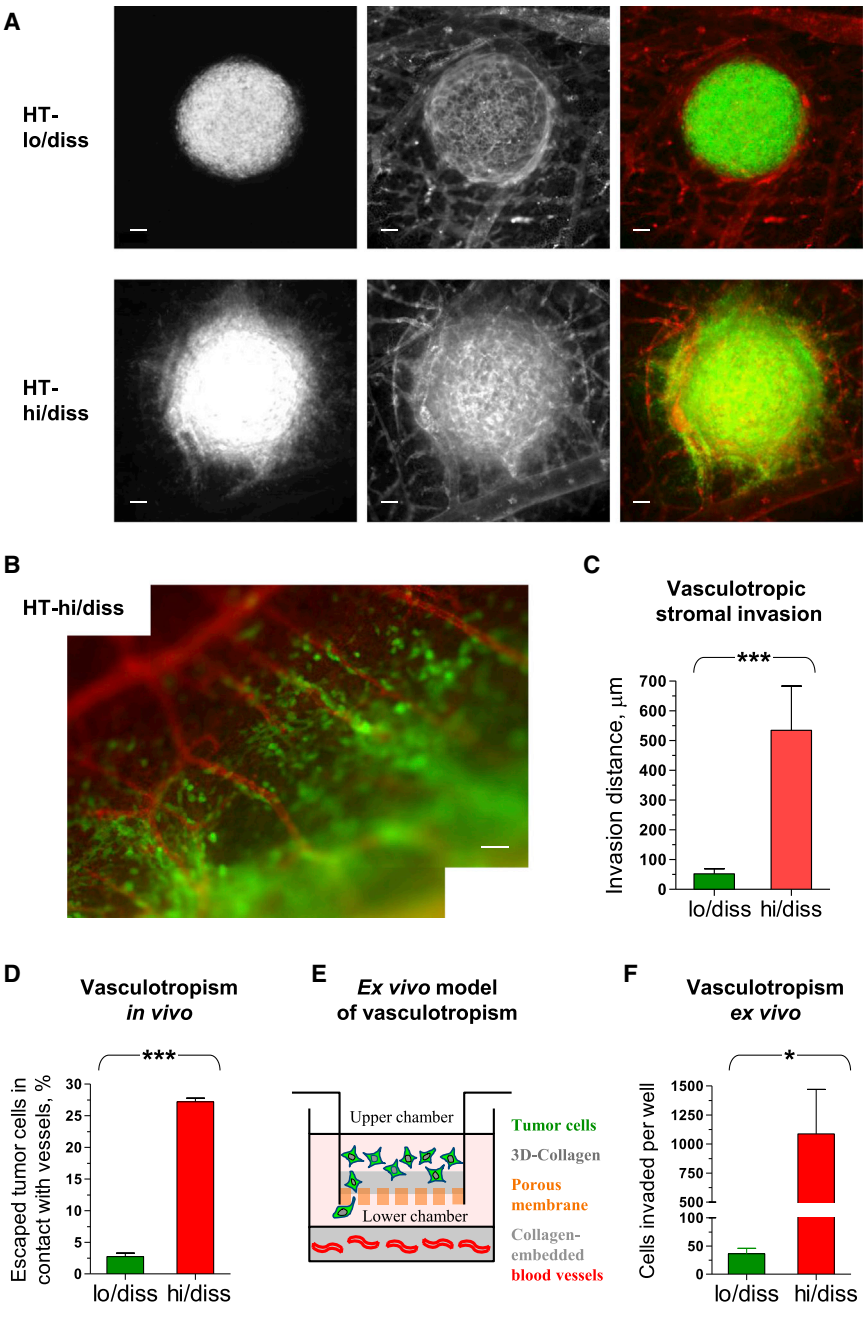

Figure 2. Quantitative Analysis of Cancer Cell Intravasation in Avian Model Systems

(A) Representative images of HT-lo/diss (top) and HT-hi/diss (bottom) primary tumors depicted in the green channel to delineate GFP-tagged tumor cells (left), red channel to visualize LCA-labeled vasculature (middle), and merged channels (right) to appreciate the entire primary tumor (green) against CAM vasculature (red). Bars, 100 μm.

(B) Vasculotropic behavior of HT-hi/diss cells. The GFP-tagged tumor cells, escaping from the primary tumor (green), appear to migrate along tumor-converging blood vessels (red). Bar, 50 μm.

(C) Quantification of vasculotropic stromal invasion from HT-lo/diss and HT-hi/diss primary tumors. $n \geq 11$ for each group. Data are shown as mean ± SEM. ***$p < 0.001$.

(D) Quantification of vasculotropic fibrosarcoma cells associated with tumor-converging blood vessels in HT-lo/diss and HT-hi/diss tumors (three independent experiments). A total of 519 cells were analyzed in the highly invasive HT-hi/diss tumors (n = 12), whereas only 65 cells were available for analysis of largely non-invasive HT-lo/diss tumors (n = 9). Data are shown as mean ± SEM. ***$p < 0.001$.

(E) Ex vivo transwell model for measuring vasculotropic behavior of tumor cells. GFP-tagged tumor cells are placed into inserts containing porous membrane occluded with native collagen. The inserts are placed into wells containing collagen-embedded blood vessels at the bottom. The cells are allowed to migrate toward chemoattractants emanated into serum-free medium from the vessels. Transmigrated GFP cells are collected and quantified.

(F) Quantification of tumor cell vasculotropism ex vivo. GFP-tagged HT-lo/diss and HT-hi/diss tumor cells that transmigrated across the collagen layer toward blood vessels were collected and quantified using immunofluorescent microscope. $n \geq 11$ for each group. Data are shown as mean ± SEM. *$p < 0.05$.

the nearest vessel lumen. Tumor cells within 2–5 μm from the center of a proximal vessel were defined as yellow-orange-red ("hot") in the color map (inset in Figure 4B, left). Correspondingly, the hot cells would comprise the tumor cells that are fully positioned within the vessel lumen (intravasated) and the tumor cells that are crossing the vessel wall (intravasating), whereas violet-blue color of tumor cells would indicate their extravascular position (Figure 4B, left).

Strikingly, when superimposed on the total tumor cell population, the majority of hot HT-hi/diss cells (i.e., intravascular or vessel wall penetrating) were localized to the primary tumor core (Figure 4B, middle). When superimposed on the total vasculature, the hot HT-hi/diss cells aligned almost exclusively with the intratumoral blood vessels and not with the vessels at the tumor border or invasive front (Figure 4B, right). A 40× zoomed image of a tumor slice, containing both tumor core and invasive outgrowth (Figure 4C), confirmed that the majority of intravascular cells were located within the tumor interior in close association with the intratumoral blood vessels (Figure 4D). Furthermore, when the Imaris-rendered 3D blood vessels are viewed in semitransparent mode, HT-hi/diss cells defined as hot by color mapping were observed either as fully or partially intraluminal (Figure 4E).

The unbiased computerized quantification of all hot HT-hi/diss cells across whole primary tumors demonstrated that the vast majority of fully or partially intravascular tumor cells were

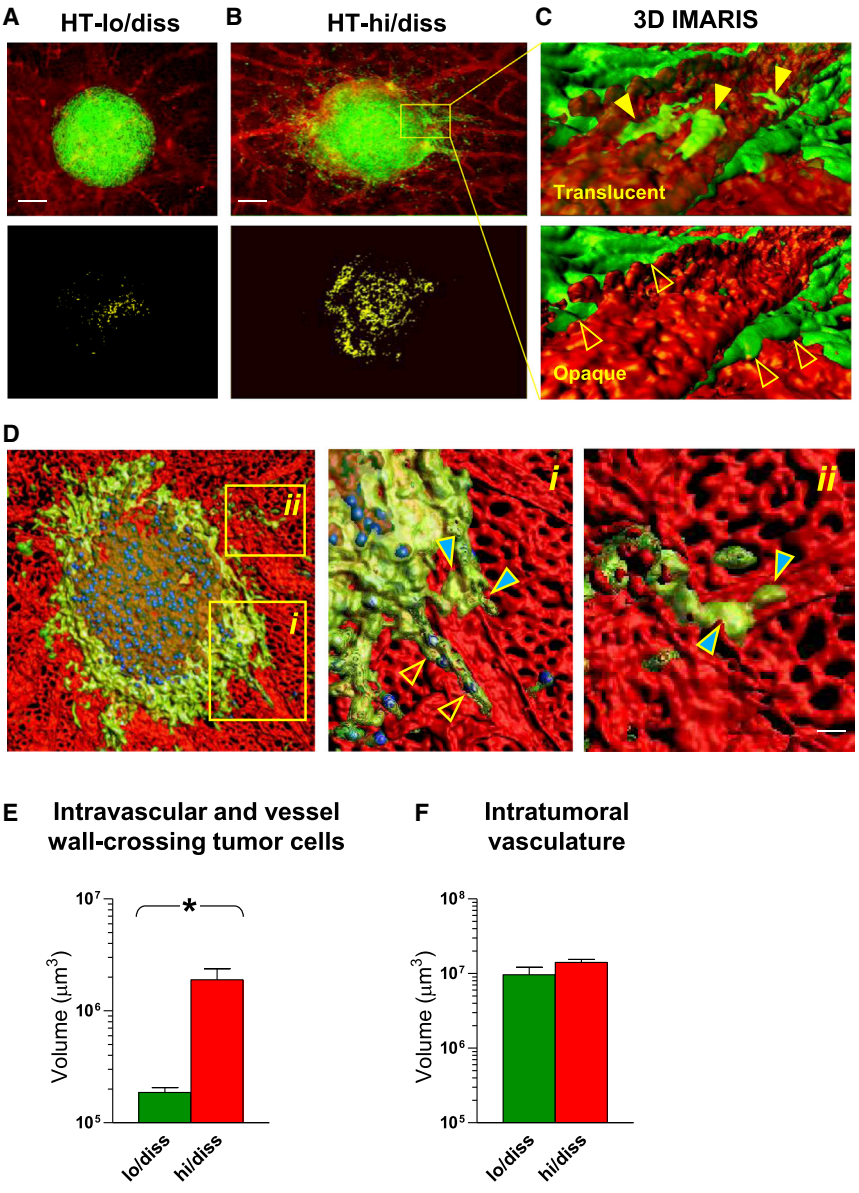

Figure 3. Discrimination between Intraluminal and Abluminal Position of Cancer Cells within the Primary Tumor

(A and B) Tumors were initiated from GFP-labeled HT-lo/diss cells (A) and HT-hi/diss cells (B). The vasculature was contrasted in vivo with Rhodamine-LCA (top). Bars, 200 μm. z stacks were acquired with a confocal microscope and rendered 3D in Imaris (bottom), allowing a conservative threshold to delineate a real colocalization signal (yellow), associated with intravascular tumor cells and tumor cells crossing vessel walls.

(C) 3D Imaris images from the area boxed in (B), depicting HT-hi/diss cells (green) and blood vessel (red) in translucent (top) or opaque (bottom) modes allowing for discrimination between intravascularly localized tumor cells (yellow arrowheads) and tumor cells located on the abluminal surface of the vessel (open arrowheads).

(D) High-resolution slice of a whole HT-hi/diss tumor imaged at 63×. Enlarged boxed areas (i and ii) on the right depict GFP-tagged tumor cells (green) appearing as entering blood vessels (blue arrowheads) or located at the abluminal surface of the vessels (open arrowheads). Bar, 5 μm.

(E and F) Total volume of tumor cells identified as intravascular or crossing vessel walls (E) and the volume of intratumoral vasculature (F) were quantified in HT-lo/diss and HT-hi/diss primary tumors (n = 4 for each tumor type). Data are shown as mean ± SEM. *p < 0.05.

localized within the interior core of a primary tumor (96.3% ± 0.7%, n = 15; p < 0.0001) and not associated with the tumor exterior, where primary tumor cells invade adjacent stroma along tumor-converging blood vessels (Figure 4F, left). We analyzed whether this striking percentage differential between hot HT-hi/diss cells within tumor interior versus invasive outgrowths could be attributed to differences in total numbers of tumor cells present in these areas. Quantification has indicated that despite its quite tight and seemingly overpopulated appearance, only 40.5% ± 4.0% of all tumor cells constituted the tumor core (Figure 4F, right), and, therefore, the very low levels of hot tumor cells beyond core borders could not be explained by putatively low numbers of escaping HT-hi/diss cells since only 3.7% ± 0.7% intravascular cells were among the 59.5% ± 4.0% of stroma-invading tumor cells.

We verified whether the tumor cells constituting the primary tumor core and the tumor cells escaping from the primary tumor had comparable potentials for intravasation into the tumor-associated vasculature. The volumes of blood vessels within and outside primary tumors were quantified (Figure 4G, left), and then the intravasation potentials, defined here as the ratios between the volume of tumor-associated blood vessels and tumor cell number, were determined separately for the inner and outer portions of individual primary tumors (Figure 4G, right). These quantifications indicated that the preferential localization of intravasation events to the tumor core (>95%) could not be attributed to either larger volume of the vasculature (Figure 4G, left) or higher numbers of tumor cells (Figure 4F, right) within the tumor core compared to the tumor exterior. In fact, the spatial potentials for intravasation were almost identical between the escaping tumor cells positioned outside tumor boundaries and the tumor cells constituting the primary tumor core (Figure 4G, right).

These results strongly indicate that our unique high-resolution confocal microscopy approach allows for unambiguous identification, localization, and computerized quantification of primary tumor cells that have intravasated or are in the process of intravasation and, correspondingly, are positioned either completely or partially within blood vessels.

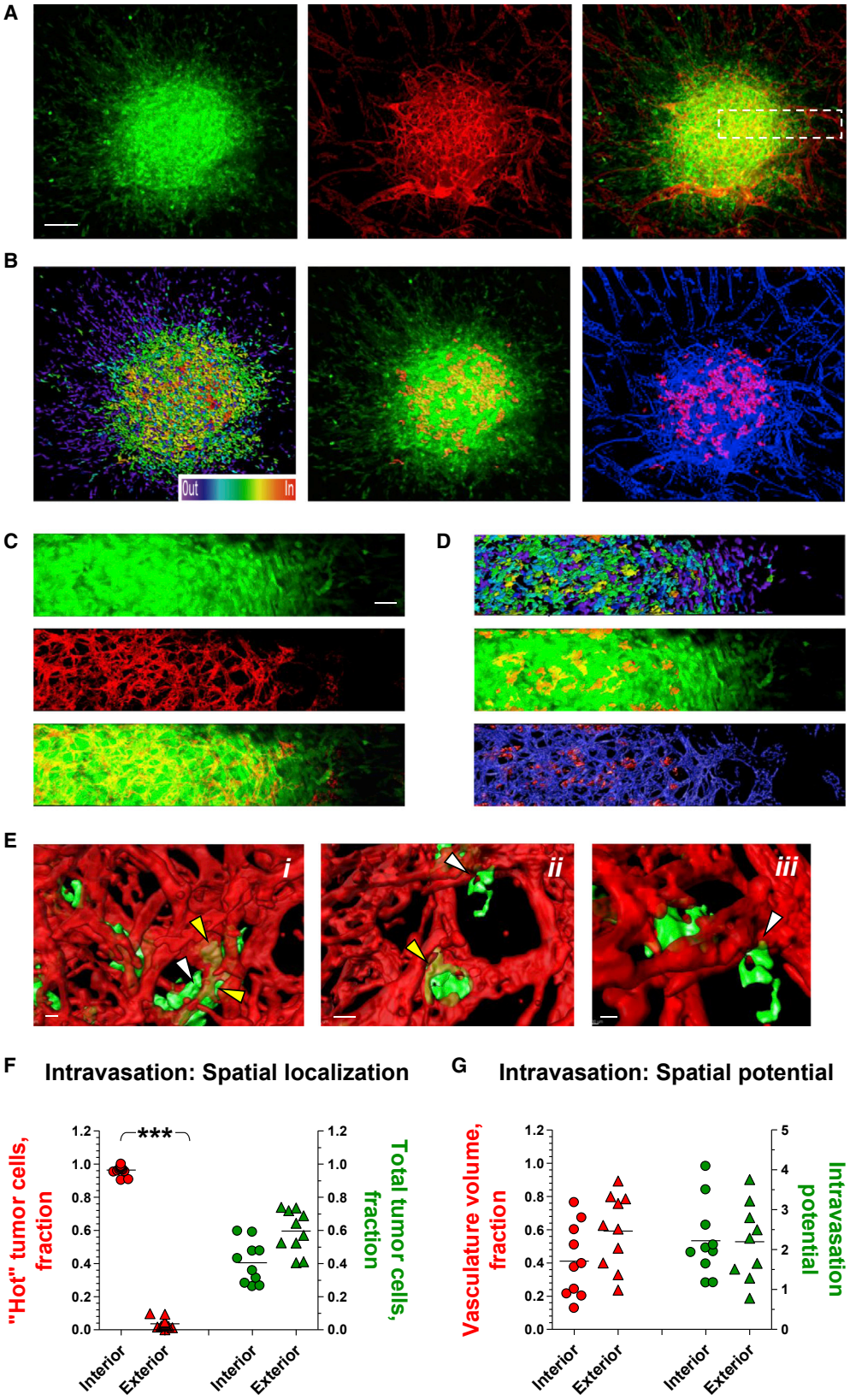

(legend on next page)

Analysis of Tumor Vasculature within the Tumor Interior versus Tumor-Adjacent Areas for Blood Vessel Permeability, Hypoxia Levels, and Tumor Cell Trapping Potential

To investigate whether the observed spatial preference for intravasation in the tumor core might be linked to the higher permeability of intratumoral vasculature, we determined the differential in the leakiness of intratumoral versus tumor-adjacent blood vessels. Permeability indices were quantified as the ratios of the levels of low-molecular-weight dextran exudation versus total volume of the vasculature highlighted by non-permeable high-molecular-weight dextran (Figure S3A). This analysis clearly demonstrated that dextran exudation occurred mainly within the tumor core since the permeability index was more than 4-fold higher for the intratumoral vasculature than for tumor-adjacent vessels (Figure S3B; $p < 0.05$). This leakiness of newly formed intratumoral blood vessels directly correlates with their ability to sustain tumor cell intravasation, linking high levels of vessel permeability with the ability of intratumoral vessels to facilitate tumor cell intravasation.

We next analyzed whether the leakiness of intratumoral vessels and their intravasation-sustaining capability were associated with high levels of hypoxia within the core of primary tumor. Tumor-bearing embryos were treated with the hypoxia probe pimonidazole, which demonstrated very low in vivo levels of hypoxia within the tumor interior and complete absence of hypoxia in the areas of tumor outgrowths into the tumor-adjacent stroma along blood vessels (Figures S4A–S4D), consistent with high levels of primary tumor vascularization and thus oxygenation at the time of intravasation analysis. Together, vessel permeability and hypoxia data indicate that tumor cell intravasation occurs within the primary tumor core via leaky, permeable vessels, which provide enough oxygenation to sustain intravasation ability of tumor cells without aid of hypoxia-induced gene expression.

We also verified whether intravascular localization of tumor cells within the primary tumor versus the tumor outgrowths might be associated with incidental or preferential trapping of tumor cells, which may have intravasated outside of the primary tumor core. Tumor cells stably expressing red fluorescent tdTomato protein were inoculated intravenously (i.v.) into embryos already bearing intramesodermal CAM tumors. Inoculated "red" tumor cells did congregate in the CAM vessels converging on GFP-labeled primary HT-hi/diss tumors but were not observed in the intratumoral vasculature (Figure S4E). Similar results also were observed in the tumors initiated from highly aggressive and invasive human epidermoid carcinoma cell line, HEp3 (Figure S4F). Furthermore, i.v. inoculations of red-labeled tumor cells into mice with large lung metastases originating from primary HT-hi/diss ear tumors also fail to demonstrate inoculated cells trapped within the GFP-labeled metastatic foci (Figure S4G). These data provide additional strong support for an intratumoral origin of the intravascular cells identified by our intravasation-scoring method.

Metastatic Potential of Cancer Cells Positively Correlates with the Numbers of Intravasation Events within Primary Tumors

To strictly delineate fully intravasated tumor cells positioned entirely within the lumen of blood vessel, the Imaris software was used first to create an isosurface-rendered tubular reconstruction of the vasculature and then to outline, mask, and solidify the tubular structures (Figure S5). This solidified signal contains signals for any intraluminal GFP-tagged tumor cells fully localized within the vasculature and excludes any signals from tumor cells positioned abluminally. By applying the threshold for a tumor cell volume, the tumor cells partially penetrating a vessel wall are also excluded from the solidified vascular mask, allowing us to identify unambiguously and to quantify truly intravascular tumor cells. These bona fide intravasated cells resided almost exclusively within the angiogenic vessels in the core of HT-hi/diss tumors (Figure 5A, lower panels). Intravasation potentials, measured as the ratios between the volume of intratumoral vasculature to the total number of cancer cells constituting a primary tumor, were then compared to intravasation indices, determined here as the ratios between the number of fully intravascular tumor cells and the volume of intratumoral vasculature. For HT-hi/diss tumors, these two parameters

Figure 4. Spatial Localization and Quantification of Intravasation Events across the Entire Primary Tumor

(A) HT-hi/diss tumors were initiated from GFP-tagged cells (left). The vasculature was highlighted in live embryos with Rhodamine-LCA (middle). Merged signals are depicted on the right. Original magnification, 20×. Bar, 200 μm.

(B) The images in (A) were rendered 3D in Imaris and processed further to assign each and all tumor cells a distinct color depending on their distance from the center of the nearest blood vessel. Left, according to the "in-out" scale on the bottom, the tumor cells localized within 2–5 μm from the lumen center fell into the yellow-red-orange (hot) category, whereas the farther-distanced tumor cells were designated as dark blue-violet. Middle, segregated "orange-red" cells were overlaid over the green signal representing all tumor cells (note that orange-red signals become yellow when merged with green signal). Right, segregated hot tumor cells were overlaid in magenta color over the signal representing total vasculature that was rendered cyan blue for clarity. Note the inner tumor core position of almost all hot cells.

(C and D) A portion of the tumor (boxed area in A) was imaged at 40× magnification and processed as described in (A) and (B), respectively. Bar, 50 μm.

(E) High-resolution (63×) 3D-Imaris-processed images were rendered translucent to visualize tumor cells localized intravascular (yellow arrowheads in i and ii) or appearing as entering blood vessels (white arrowheads in mutually rotated images ii and iii). Bars, 10 μm.

(F) Hot tumor cells (scattergrams on the left) and total tumor cells (scattergrams on the right) were quantified in different portions of primary tumors, namely, in the inner core (interior) and invasive outgrowths along blood vessels (exterior). Data points are fractions of intraluminal hot or total tumor cells in the interior or exterior of individual tumors ($n = 15$).

(G) Intravasation potential of tumor cells localized to the interior or exterior of primary tumors. Volumes of vasculature associated with the indicated tumor portion are presented as a fraction of total signal associated with the solidified vasculature (scattergrams on the left). Intravasation potential was quantified as the ratio between the volume of the vasculature and the number of tumor cells in the indicated area of the primary tumor and is expressed in arbitrary units (scattergrams on the right). Data points represent individual tumors ($n = 10$). ***$p < 0.001$.

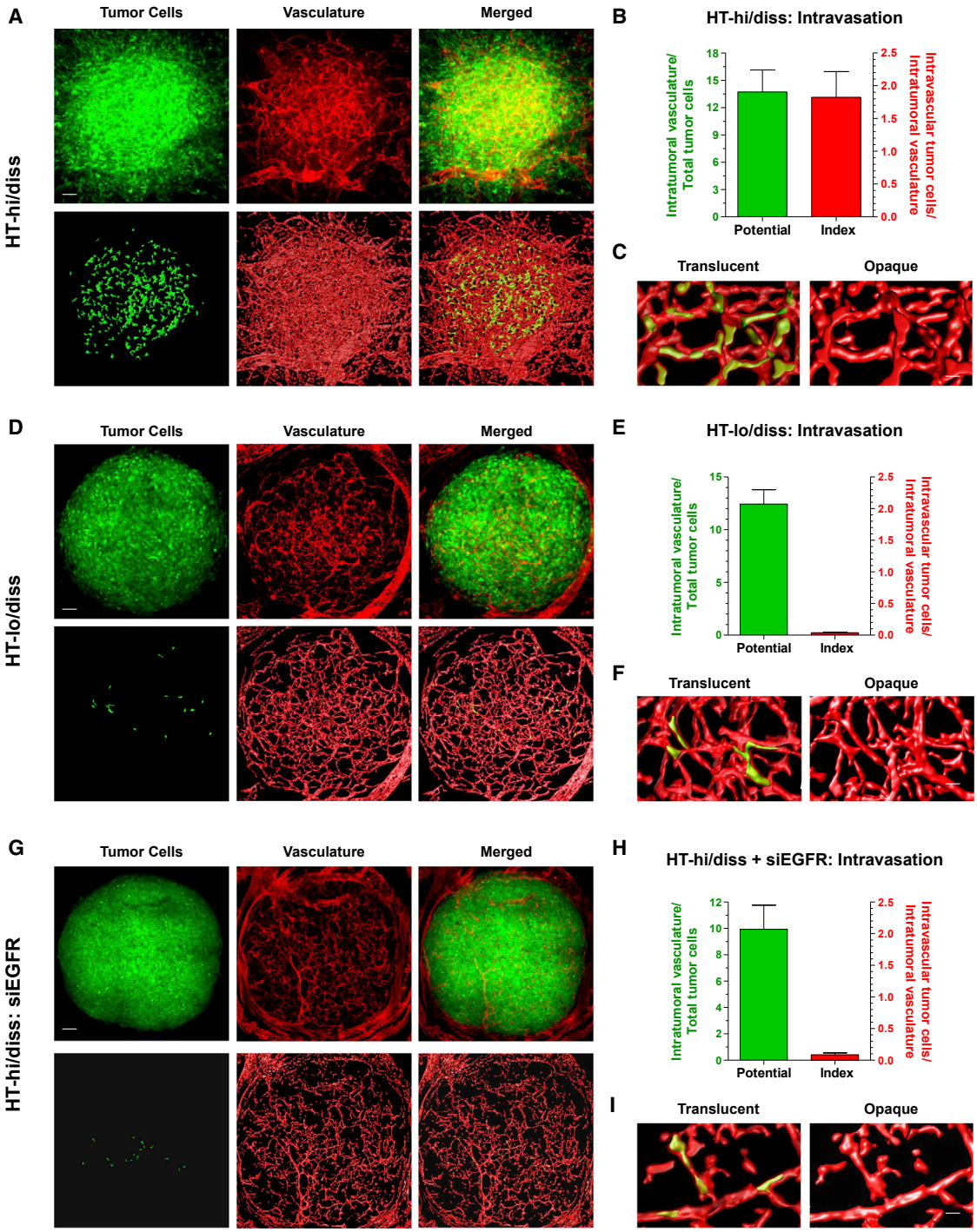

Figure 5. Intravasation Efficiency Correlates with the Metastatic Potential of Tumor Variants and Depends on EGFR Expression

Tumors were initiated from GFP-tagged HT-hi/diss cells (A–C; n = 10), HT-lo/diss cells (D–F; n = 5), and HT-hi/diss cells treated with siEGFR (G–I; n = 10).

(A, D, and G) The original signals for tumor cells (green) and the vasculature (red) and merged channels are presented on the top. The signals for segregated intravascularly localized tumor cells, the 3D-rendered vasculature, and their colocalization are presented at the bottom. Bars, 100 μm.

(B, E, and H) Intravasation potentials of tumor cell variants (green bars on the left) were quantified as the ratios between the volume of intratumoral vasculature and the total number of primary tumor cells. Intravasation indices (red bars on the right) were calculated for individual tumors as the ratios of segregated intravascularly positioned tumor cell numbers to the volume of intratumoral vasculature. Both parameters are expressed in arbitrary units. Data are shown as mean ± SEM.

(C, F, and I) The translucent and opaque modes of high-resolution images verify the intravascular localization of segregated tumor cells. Bars, 25 μm.

constituted 13.7 ± 7.7 and 1.8 ± 0.4 in arbitrary units (Figure 5B, green versus red bars).

Our stringent intravasation-scoring approach confirmed the low intravasation capacity of HT-lo/diss tumors. Thus, only a few tumor cells were located intravascularly despite the similar size of HT-lo/diss microtumors (Figure 5D, lower panels). Although the intratumoral vessel core developed in HT-lo/diss tumors was less dense than in HT-hi/diss tumors, the overall intravasation potential of HT-lo/diss cells was not significantly different from HT-hi/diss cells (Figure 5E, green bar). However, the intravasation index of HT-lo/diss cells was substantially lower than that of HT-hi/diss cells (Figure 5E, red bar). This more than 40-fold differential in the intravasation indices between HT-lo/diss and HT-hi/diss variants ($p < 0.01$) was in full agreement with the 50- to 100-fold differentials in their metastatic abilities demonstrated previously in independent spontaneous metastasis models (Deryugina et al., 2005; Partridge et al., 2007). Importantly, the translucent versus opaque modes of Imaris-rendered 3D reconstructions validated the actual intravascular position of tumor cells identified as intravasated in both HT-hi/diss and HT-lo/diss tumors (Figures 5C and 5F).

EGFR Is a Molecular Factor Required for Intratumoral Intravasation

Our previous studies have linked high intravasation capability of HT-hi/diss cells with their heightened expression of EGFR as compared to HT-lo/diss cells (Minder et al., 2015). Herein, the involvement of EGFR in intratumoral intravasation was mechanistically analyzed with a small interfering RNA (siRNA)-mediated loss-of-function approach. Either control siRNA construct (siCtrl) or siRNA against EGFR (siEGFR) did not affect substantially the growth of primary HT-hi/diss tumors compared to untreated HT-hi/diss cells, but siEGFR treatment substantially reduced the invasion ability of HT-hi/diss cells (Figures S6 and 5G, upper left). In addition, siEGFR negatively affected the development of fully interconnected intravascular vessel networks (Figure 5G, upper middle), which coincided with a remarkable reduction in the population of fully intravascular tumor cells (Figure 5G, lower panels). When quantified, there was a 20-fold decrease in the intravasation indices within siEGFR tumors compared to HT-hi/diss control ($p < 0.001$) (Figure 5H, red bar), although the intravasation potential of EGFR-deficient HT-hi/diss cells was only slightly diminished (green bars in Figures 5H versus 5B). The translucent and opaque modes of 3D imaging again confirmed the luminal position of the very few intravasated HT-hi/diss cells in siEGFR tumors (Figure 5I).

Side-by-side quantitative comparisons demonstrated a substantial reduction in the actual numbers of fully intravascular tumor cells within EGFR-silenced HT-hi/diss tumors as well as in HT-lo/diss tumors compared to HT-hi/diss control (Figure 6A). Importantly, these low numbers of true intraluminal tumor cells could not be attributed to significantly smaller vascular beds since the volumes of intratumoral vasculature were very similar between all three tumor types (Figure 6B). However, the intravasation levels strongly and positively correlated with EGFR protein expression, which was naturally low in HT-lo/diss cells and almost negative in siEGFR-treated HT-hi/diss cells (Figure 6C). These EGFR-dependent intravasation patterns also correlated with the dissemination potentials of HT-lo/diss, HT-hi/diss, and siEGFR-treated HT-hi/diss cells as measured in the spontaneous metastasis model by human *Alu*-qPCR. Thus, HT-lo/diss cells demonstrated a near complete lack of intravasation, whereas EGFR-deficient HT-hi/diss cells manifested a dramatically inhibited intravasation relative to HT-hi/diss control (Figure 6D), although all three cell types generated primary tumors of comparable sizes (Figure 6E).

To investigate whether the spatial preference for intratumoral intravasation correlates with a differential activity of EGFR in tumor cells localized to the core of a primary tumor versus its stroma-invasive tumor outgrowths, we conducted immunostaining for phosphorylated EGFR (pEGFR) in GFP-tagged HT-hi/diss tumors. The staining for pEGFR was associated mainly with tumor cells localized within the core of primary tumors, whereas tumor outgrowths into the stroma appear mostly negative for pEGFR despite their positive staining for total EGFR (Figure 6F), indicating that tumor cell intravasation within the tumor interior might critically depend on EGFR activity.

Intratumoral and EGFR-Dependent Intravasation of Human Carcinoma Cells

By employing HEp3 carcinoma cells, we next verified whether intratumoral localization of intravasation observed in the fibrosarcoma primary tumors would also be attributable to an epithelial cancer model. Our automated quantification throughout whole-mounted primary tumors analyzed by Imaris mapping demonstrated that 86.4% ± 2.9% of all intravascularly positioned HEp3 cells were localized to the tumor interior ($n = 9$; $p < 0.001$). When analyzed by the Imaris-3D mask assay, the percentage of intravasated hot cells identified outside of the primary tumor core constituted only 2.6% ± 0.2% (Figure 7A), which was comparable with the results for HT-hi/diss fibrosarcoma (Figure 4F).

To address the role of EGFR in the intravasation process within primary carcinomas, we compared the effects of EGFR deficiency caused by treatment of HEp3 cells with siEGFR. Neither control siCtrl nor siEGFR affected the overall development of HEp3 tumors compared to non-treated control (Figure S7). In contrast to HT-hi/diss fibrosarcoma, siEGFR treatment did not cause significant diminishment in adjacent stroma invasion by HEp3 tumors (compare Figures 5G versus 7B and Figure S6 versus S7), emphasizing that the specific effects of EGFR downregulation could be different in tumor types of different tissue origin. However, similar to HT-hi/diss tumors, the downregulation of EGFR (Figure 7B, inset) dramatically diminished the percentage of intravascular cells in HEp3 primary tumor as measured by Imaris mapping or by 3D-mask assay ($p < 0.0001$) (Figure 7B). Similar to EGFR-deficient HT-hi/diss tumors, downregulation of EGFR in HEp3 tumors did not change the total volume of intratumoral vasculature (Figure 7C) but significantly reduced the interconnectivity of intratumoral blood vessels (Figure 7B). Finally, HEp3 intravasation patterns as revealed microscopically in our 3D-mask segregation method (Figures 7A and 7B) correlated directly with the numbers of intravasated HEp3 cells measured by *Alu*-qPCR in the spontaneous intravasation assay. Thus, EGFR silencing resulted in a dramatic inhibition of HEp3 cell intravasation capacity compared to the

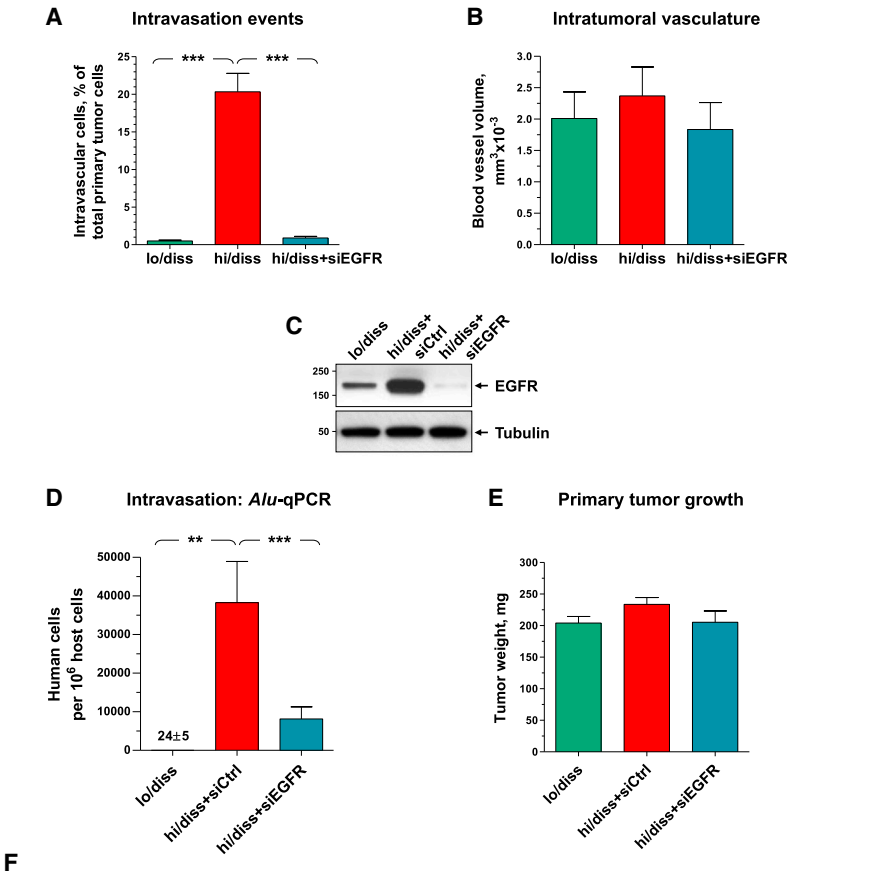

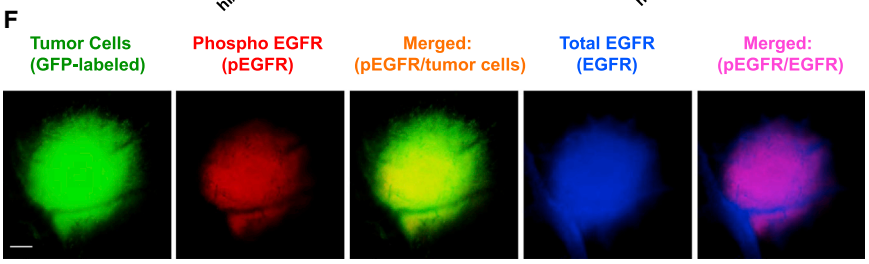

Figure 6. Comparative Analysis of Intravasation Capabilities of Tumor Variants Relative to Expression of EGFR Protein

(A and B) Tumors, initiated from GFP-tagged HT-lo/diss cells (n = 7) and HT-hi/diss cells, untreated (n = 14) and treated with siEGFR (n = 11), were analyzed as entire units for the number of intravascular tumor cells (A) and the volume of intratumoral vasculature (B). Data are shown as mean ± SEM. ***$p < 0.001$.

(C) Analysis of EGFR protein expression in HT-lo/diss, HT-hi/diss cells 4 days after treatment with control (siCtrl) and EGFR-specific (siEGFR) siRNA. Below, α-tubulin is shown as protein-loading control. Position of molecular weight markers is indicated on the left.

(D and E) Primary tumors were initiated in ovo from GFP-tagged HT-lo/diss cells (n = 11) and HT-hi/diss cells, treated with control siRNA (siCtrl; n = 47) or siEGFR (n = 29). Embryos were analyzed by human *Alu*-qPCR for the number of intravasated tumor cells trapped in the CAM vasculature (D) and tumor growth (E). Data are shown as mean ± SEM. **$p < 0.01$; ***$p < 0.001$.

(F) Intramesodermal primary tumors, initiated from GFP-labeled HT-hi/diss tumor cells, were stained on day 5 for phospho EGFR (pEGFR) and total EGFR. Signals for green (GFP), red (pEGFR), and far red (total EGFR, depicted here in blue) fluorescence were acquired monochromatically and then "colored" and merged using Adobe Photoshop software. Bar, 200 μm.

treatments with either GFP siRNA or control siRNA ($p < 0.05$ and < 0.01, respectively) (Figure 7D) but did not affect overall development and size of primary tumors (Figure 7E).

When analyzed for the activity of EGFR in different areas, primary HEp3 tumors demonstrated preferential staining for pEGFR within the primary tumor and not in the tumor cell trails invading adjacent stroma (Figure 7F). Together with the data in HT-hi/diss tumors, these results suggest that the preferential intratumoral localization of intravasation is associated with heightened activity of EGFR in primary tumors of different tissue origin.

In conclusion, by quantifying the intravasation process in a human carcinoma and human fibrosarcoma in the mouse ear and chick embryo tumor models, we have demonstrated that intravasation events are not prevalent in the invasive tumor outgrowths at the leading edge of stroma-invading primary tumors, but rather tumor cell intravasation occurs almost exclusively *within* the primary tumor core in these models.

DISCUSSION

To compensate for an overall inefficient process of metastasis, cancer cells at the primary tumor site should sustain high rates of intravasation. According to conventional views, primary epithelial tumor cells first undergo EMT, invade the adjacent stroma, migrate toward and along tumor-coalescing blood vessels, and then cross the vessel endothelium and enter the circulation (Kalluri and Weinberg, 2009). The view that stromal invasion is a prerequisite for hematogenous spreading of cancer remains prevalent in both clinical staging and basic cancer biology, and, therefore, the invasive edge of the primary tumor is still considered a major locale where metastatic cells intravasate (Ye and Weinberg, 2015).

In this study, we sought to establish spatial localization of the intravasation process and demonstrate precisely where tumor cell intravasation takes place, namely, at the invasive edge of primary tumor within the stroma-invading outgrowths or, alternatively, within the interior core of a primary tumor. This challenging task has been hindered by a severe deficiency in microscopic methods for direct quantification of intravasation events within the primary tumor, reflected in the widespread use of indirect and retrospective analyses of intravasation including measurements of tumor cells in the circulation, tumor cell colonies growing after plating peripheral blood from cancer patients (Ye

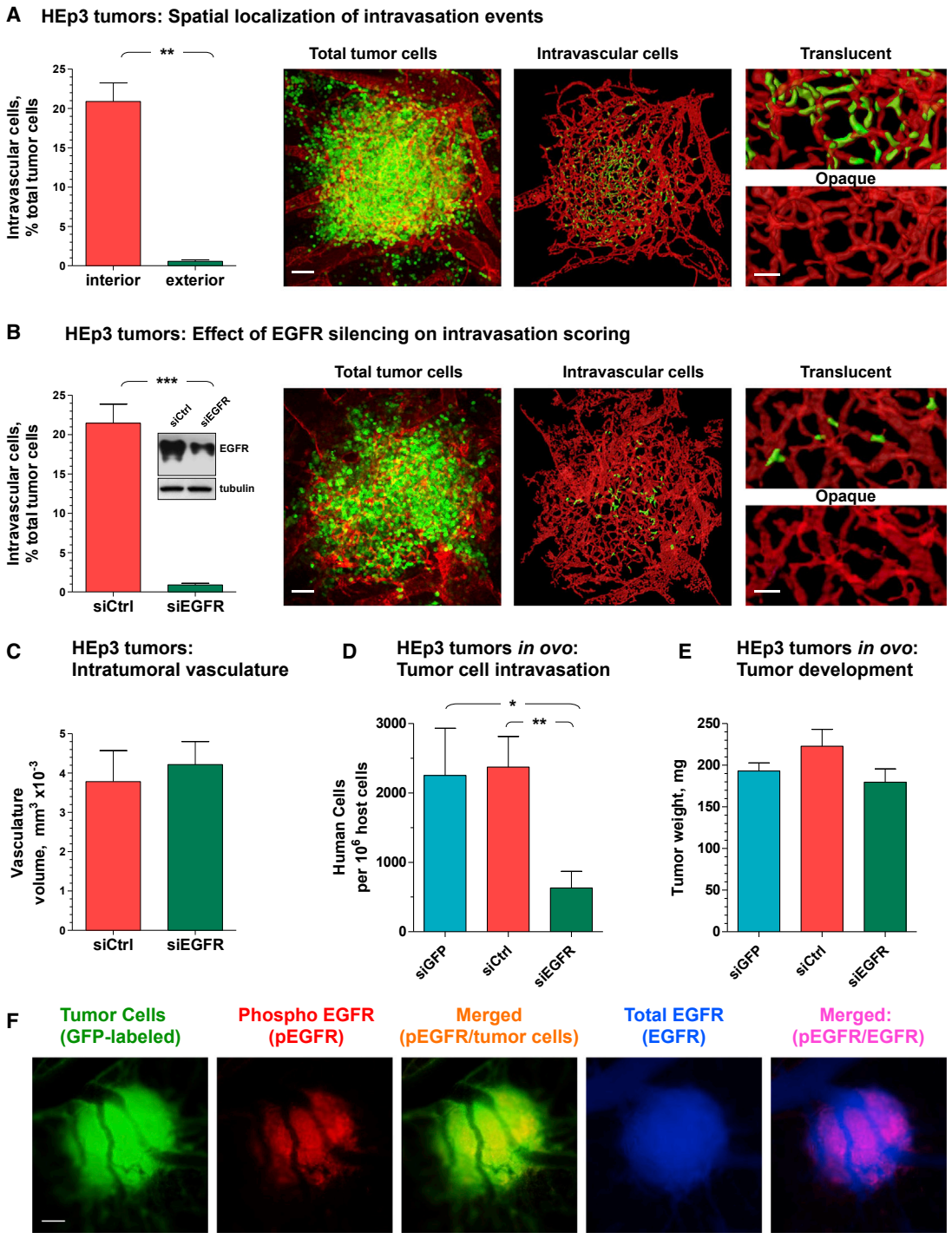

Figure 7. Intratumoral and EGFR-Dependent Intravasation of Human Carcinoma Cells

(A) Tumors were initiated from GFP-tagged HEp3 cells (n = 4) and analyzed as entire units. Bar graph, intravascular tumor cells localized either within the core of primary tumors (interior) or outside of tumor borders (exterior) were quantified as a percentage of total tumor cells. Data are shown as mean ± SEM. **p < 0.01. Representative image on the left depicts a HEp3 tumor against LCA-highlighted CAM vasculature (merged signals). The middle image depicts segregated tumor cells localized within the tumor vasculature. Bar, 100 μm. Images on the right depict intratumoral blood vessels harboring fully intravasated tumor cells, which are visible in translucent mode and become invisible when vessel surface is made opaque. Bar, 25 μm.

(B) Tumors were initiated from GFP-tagged HEp3 cells treated with control siRNA (siCtrl; n = 4) or siEGFR (n = 11). Bar graph, intravascular tumor cells were quantified as a percentage of total tumor cells. Data are shown as mean ± SEM. ***p < 0.001. Inset, expression of EGFR protein (~180 kDa) was analyzed by western blotting 5 days after siRNA cell transfections. Below, α-tubulin (~50 kDa) is shown as protein-loading control. Image on the left depicts a siEGFR-HEp3

(legend continued on next page)

and Weinberg, 2015) and tumor-bearing mice (Giampieri et al., 2009; Gligorijevic et al., 2012; Ramirez et al., 2011), or primary tumor cells arrested within the capillary system (Deryugina and Quigley, 2008; Kim et al., 1998). Adding to this complexity is the intra-tumor heterogeneity of primary tumors with regard of cell motility and rates of intravasation in different areas (Egeblad et al., 2010; Giampieri et al., 2009). Although a few microscopic methods involving live-animal imaging have been introduced to visualize rare tumor cells in the act of intravasation (Harney et al., 2015; Kedrin et al., 2008; Wyckoff et al., 2007), only small areas of primary tumors can be visualized, and, therefore, quantification of intravasation events across a whole primary tumor has never been conducted.

To quantify the process of intravasation and to uncover the preferential place for intravasation, we developed unique methods to score intravasation events across the entire primary tumor and applied these methods to highly invasive human tumor variants of distinct histological origin, namely, aggressive human fibrosarcoma (HT-hi/diss) and carcinoma (HEp3), employed in different animal models. Whole-mounted primary tumors, represented both by an interior core and invasive trails along tumor-converging blood vessels, were analyzed by fully automated intravasation-scoring approaches discriminating in an unbiased manner between the abluminal (outside the vessel wall), subluminal (partially penetrating the vessel wall), or intraluminal (fully within the vessel) position of each and all cancer cells constituting the entire primary tumor. This direct and unbiased methodology led us to the key finding that the vast majority of intravasation events (90%–95%) were localized to the inner core of invasive primary tumors. Regardless of which of two distinct scoring methods was used for quantification of intravasation events, less than 10% of all intravasation events were localized to the invasive trails formed by tumor escapees. Therefore, our study indicates that the intravasation process might not rely on invasive vasculotropic tumor cells escaping the primary tumor, invading the adjacent stroma, and migrating along tumor-associated blood vessels. Instead, our study challenges a conventional notion that the invasive edge is a preferential locale for tumor cell intravasation and implies that primary tumor cells actively enter the intratumoral vasculature probably early and in parallel to and independent of tumor cell invasion into adjacent stroma.

It might be suggested that tumor cells in the invasive outgrowths enter tumor-coalescing blood vessels more frequently than tumor cells within the tumor and are carried away more efficiently via tumor-coalescing vessels since these vessels are less torturous and therefore have better blood circulation. If true, more tumor cells should be scored as crossing the vessel wall in the invasive outgrowths by our encompassing intravasation-mapping method. However, this analysis did not provide any evidence of a significant population of tumor cells that would be scored as entering blood vessels outside the tumor core, thus further arguing against substantial intravasation outside of primary tumor core.

Mechanistically, we demonstrated that EGFR is a requisite molecular factor critical for tumor cell intravasation. This focus on an important cancer-related protein was driven by our recently established multimolecular axis involving tumor cell EGFR, tumor-derived interleukin-8 (IL-8), and host-derived, VEGF-liberating, neutrophil MMP-9, the molecules that together regulate the development, structural integrity, and the permeability of an intravasation-supporting vasculature and ultimately determine the levels of intravasation (Minder et al., 2015). In the present study, the low levels of total EGFR expression, occurring either naturally in non-aggressive tumor cells or caused by intended downregulation of EGFR expression, were associated with dramatically decreased numbers of intravasation events scored by our more stringent scoring method detecting only intravascular tumor cells. In the case of siEGFR-treated HT-hi/diss cells, this diminishment of intravasation could have also been associated with their reduced motility in vivo. This cell-motility-regulating function of EGFR would be consistent with its known role in cancer biology (Arteaga and Engelman, 2014; Kovacs et al., 2015) and in cell intravasation (Xue et al., 2006). However, similar EGFR deficiency did not affect stroma invasion of primary HEp3 tumors yet substantially diminished their intravasation, a finding that may reflect lower sensitivity to EGFR suppression of epithelial origin carcinomas compared to mesenchymal origin fibrosarcomas.

Importantly, our study points to a role for EGFR in the regulation of intravasation. Thus, we have demonstrated that in both fibrosarcoma and carcinoma tumor types, EGFR deficiency resulted in the formation of structurally impaired and disjointed intratumoral vasculature, which would preclude the efficient entry of EGFR-deficient tumor cells even if they were motile. Furthermore, even if tumor cells had entered such compromised vasculature, those intravasated cells would likely remain physically trapped within the tumor core rather than carried away with blood flow. Therefore, our study points to a specific role of EGFR in tumor cell intravasation, namely, regulation of the development in vivo of intravasation-sustaining vasculature, and this role of EGFR is independent of its established roles in regulating cancer cell proliferation, survival, and EGF-mediated motility (Xue et al., 2006).

tumor against LCA-highlighted CAM vasculature (merged signals). The middle image depicts segregated tumor cells localized within the tumor vasculature. Bar, 100 μm. Images on the right depict intratumoral blood vessels in translucent or opaque modes. Bar, 25 μm.

(C) Volumes of intratumoral vasculature within siCtrl and siEGFR HEp3 tumors were quantified after solidifying 3D-Imaris reconstructions. Data are shown as mean ± SEM.

(D and E) Primary tumors were initiated in ovo from the GFP-tagged HEp3 cells treated with either of two different control siRNA constructs, siGFP (n = 9) or siCtrl (n = 8), or siEGFR (n = 10). Embryos were analyzed by human *Alu*-qPCR for the number of intravasated tumor cells localized in the CAM vasculature (D) and tumor growth (E). Data are shown as mean ± SEM. *$p < 0.05$; **$p < 0.01$.

(F) Intramesodermal primary tumors, initiated from GFP-labeled HEp3 tumor cells, were stained on day 7 for phospho EGFR (pEGFR) and total EGFR. Signals for green (GFP), red (pEGFR), and far red (total EGFR, depicted here in blue) fluorescence were acquired monochromatically and then colored and merged using Adobe Photoshop software. Bar, 200 μm.

Our data also suggest that the activity of EGFR, which is higher in the core of the primary tumor compared to the stroma-invasive tumor outgrowths, could dictate a spatial preference for the intratumoral localization of the intravasation process. Such heightened intratumoral EGFR activity could be induced by tumor cell-vascular cell interactions, and, therefore, a high density of neovasculature within the core of a primary tumor might also facilitate EGFR-dependent intratumoral intravasation. These observations are consistent with our published results and findings from other laboratories indicating the importance of EGFR for the integrity and permeability of blood vessels (Blouw et al., 2015; Deryugina and Quigley, 2015; Minder et al., 2015). Therefore, our approaches have been instrumental not only in linking EGFR expression to the process of tumor cell intravasation per se, but also in demonstrating an additional role for EGFR in cancer, that is, EGFR-regulated development of a unique, intravasation-sustaining vasculature.

This study presents quantitative evidence that can lead to reconsideration of *when* and *where* early steps of tumor cell metastasis take place. According to a conventional model (Figure 1H, left), the majority of intravasation events are expected to be within tumor-converging blood vessels (co-opted or newly formed during the invasive stage), at or beyond the primary tumor boundaries. Alternatively, the bulk of intravasation events could be localized within the new immature blood vessels developing in the interior core of the primary tumor (Figure 1H, right). The key findings of this study support the latter concept and indicate that the intravasation process could be uncoupled from the formation of the invasive leading edge. This concept of preferential intravasation within the tumor interior is also supported by our studies demonstrating that intratumoral HT-hi/diss or HEp3 cells can retain their intravasation competence in a specific in vivo setting, where primary microtumors develop without any significant invasion into surrounding stroma (Deryugina, 2016; Juncker-Jensen et al., 2013; Minder et al., 2015).

The concept of intratumoral localization of the intravasation events implies that the intravasation process could be initiated as soon as the first angiogenic vessels are formed within the expanding tumor. During carcinoma development, this specific time period coincides with the breaching of epithelial basement membrane and the formation of the initial invasive edge (Weinberg, 2013). This ''breaching'' event, allowing the activated endothelial cells to enter the interior of an early-stage tumor and eventually generate an intratumoral angiogenic network occurs well before extensive stromal invasion observed in late-stage primary tumors in cancer patients. Our findings support this scenario and suggest that the main requirements for tumor cell dissemination via vascular routes could be an intrinsic ability of metastasis-initiating cancer cells to enter the intratumoral permeable blood vessels and the development of these vessels in the core of a growing primary tumor. Both restrictions could be therapeutically targeted and, therefore, are in the focus of our ongoing research aiming to identify those molecular characteristics of malignant cells that determine their ability to intravasate into blood vessels developing in the inner core of primary tumors. To prevent dissemination of metastasis-initiating cancer cells at the apex of their dissemination route, it would be important to identify therapeutically targetable molecular factors, tumor- or stroma-derived, governing the development of structurally sound but permeable intratumoral angiogenic vessels.

EXPERIMENTAL PROCEDURES

Cell Culture

The murine melanoma B16-F10 cell line was obtained from ATCC. The HT-hi/diss and HT-lo/diss cell variants were selected from the human HT-1080 fibrosarcoma (ATCC) for high and low levels of dissemination, respectively (Deryugina et al., 2005). Detailed description of the human head and neck epidermoid carcinoma HEp3 can be found in Juncker-Jensen et al. (2013). GFP-tagged tumor cells were described previously (Juncker-Jensen et al., 2013; Minder et al., 2015). Details of cell culture and EGFR silencing are provided in Supplemental Experimental Procedures.

Tumor Models

All research involving live animals complied with protocols approved by The Scripps Research Institute (TSRI) Committee of Animal Care.

Mouse Ear Model

GFP-tagged tumor HT-hi/diss and HT-lo/diss cells were inoculated (~5 μL of a 1×10^7 cells/mL cell suspension) into the ear dermis of NOD-SCID mice. To highlight the vasculature, tumor-bearing mice were injected i.v. with TRITC-conjugated dextran and sacrificed within 10 min. Primary tumors were excised and processed for microscopic examinations as whole mounts. The lymph nodes and lungs were analyzed by quantitative human-specific *Alu*-PCR (*Alu*-qPCR) as described (Deryugina et al., 2014).

Chick Embryo Intramesodermal Model

GFP-tagged human tumor cells were inoculated into the CAM mesoderm of chicken embryos (Deryugina and Quigley, 2008). After 5 days, embryos were injected i.v. with the Rhodamine-conjugated *Lens culinaris* agglutinin (LCA; Vector). Tumor-containing portions of the CAM were examined in immunofluorescent microscope (Olympus), fixed in formalin, and embedded into ProlongGold solution (Life Technologies) for further examinations in a confocal microscope (Zeiss), as described in Supplemental Experimental Procedures.

Confocal Microscopy Acquisition and Image Analysis

Intramesodermal tumors were initiated from GFP-labeled tumor cells. Prior to fixation, the vasculature of live embryos was contrasted with LCA. Tumor-containing portions of the CAM were fixed, and cell nuclei were stained with NucBlue (Molecular Probes). Maximum projection images of individual microtumors and tumor-adjacent areas were prepared from z stacks acquired with a confocal Zeiss microscope at 20× or 40×. The z stacks were stitched and rendered 3D to outline and mask the volume of signals for total vasculature and tumor cells. Intravasation-scoring methods are fully described in the Supplemental Information. In brief, the first method identifies and quantifies intravasating and intravascularly positioned tumor cells based on the distance between the tumor cell and the center of the lumen of the nearest blood vessel. The second method identifies and quantifies only those tumor cells that are fully localized within the luminal space.

Statistics

Where indicated, the data from individual experiments were normalized relative to the control of a particular experiment, pooled, and analyzed for statistical significance. Comparisons between two groups were conducted with a two-tailed Student's t test. A p value <0.05 was considered statistically significant.

SUPPLEMENTAL INFORMATION

Supplemental Information includes Supplemental Experimental Procedures and seven figures and can be found with this article online at http://dx.doi.org/10.1016/j.celrep.2017.03.064.

AUTHOR CONTRIBUTIONS

E.I.D. designed the study, conducted the experiments, developed the intravasation-scoring methodology, analyzed the data, and wrote the paper. W.B.K. developed the intravasation-scoring methodology and acquired and analyzed confocal microscopy data.

ACKNOWLEDGMENTS

The authors thank J.P. Quigley for critical review of this manuscript and insightful discussions. We thank Chenxing Li for her excellent technical assistance. We also thank Ewa Zajac, Petra Minder, and Ivo Rimann for their help with some of the cell transfections and chick embryo experiments. This study was supported by NIH grants R01CA105412, R01CA129484, and R01CA157792.

Received: August 18, 2016
Revised: January 29, 2017
Accepted: March 21, 2017
Published: April 18, 2017

REFERENCES

Arteaga, C.L., and Engelman, J.A. (2014). ERBB receptors: From oncogene discovery to basic science to mechanism-based cancer therapeutics. Cancer Cell *25*, 282–303.

Blouw, B., Patel, M., Iizuka, S., Abdullah, C., You, W.K., Huang, X., Li, J.L., Diaz, B., Stallcup, W.B., and Courtneidge, S.A. (2015). The invadopodia scaffold protein Tks5 is required for the growth of human breast cancer cells in vitro and in vivo. PLoS ONE *10*, e0121003.

Bobek, V., Kolostova, K., Pinterova, D., Kacprzak, G., Adamiak, J., Kolodziej, J., Boubelik, M., Kubecova, M., and Hoffman, R.M. (2010). A clinically relevant, syngeneic model of spontaneous, highly metastatic B16 mouse melanoma. Anticancer Res. *30*, 4799–4803.

Chiang, S.P., Cabrera, R.M., and Segall, J.E. (2016). Tumor cell intravasation. Am. J. Physiol. Cell Physiol. *311*, C1–C14.

Cochet, A., Dygai-Cochet, I., Riedinger, J.M., Humbert, O., Berriolo-Riedinger, A., Toubeau, M., Guiu, S., Coutant, C., Coudert, B., Fumoleau, P., and Brunotte, F. (2014). ^{18}F-FDG PET/CT provides powerful prognostic stratification in the primary staging of large breast cancer when compared with conventional explorations. Eur. J. Nucl. Med. Mol. Imaging *41*, 428–437.

Conn, E.M., Botkjaer, K.A., Kupriyanova, T.A., Andreasen, P.A., Deryugina, E.I., and Quigley, J.P. (2009). Comparative analysis of metastasis variants derived from human prostate carcinoma cells: Roles in intravasation of VEGF-mediated angiogenesis and uPA-mediated invasion. Am. J. Pathol. *175*, 1638–1652.

Coumans, F.A., Siesling, S., and Terstappen, L.W. (2013). Detection of cancer before distant metastasis. BMC Cancer *13*, 283.

Deryugina, E.I. (2016). Chorioallantoic membrane microtumor model to study the mechanisms of tumor angiogenesis, vascular permeability, and tumor cell intravasation. Methods Mol. Biol. *1430*, 283–298.

Deryugina, E.I., and Quigley, J.P. (2008). Chick embryo chorioallantoic membrane model systems to study and visualize human tumor cell metastasis. Histochem. Cell Biol. *130*, 1119–1130.

Deryugina, E.I., and Quigley, J.P. (2015). Tumor angiogenesis: MMP-mediated induction of intravasation- and metastasis-sustaining neovasculature. Matrix Biol. *44-46*, 94–112.

Deryugina, E.I., Zijlstra, A., Partridge, J.J., Kupriyanova, T.A., Madsen, M.A., Papagiannakopoulos, T., and Quigley, J.P. (2005). Unexpected effect of matrix metalloproteinase down-regulation on vascular intravasation and metastasis of human fibrosarcoma cells selected in vivo for high rates of dissemination. Cancer Res. *65*, 10959–10969.

Deryugina, E.I., Zajac, E., Juncker-Jensen, A., Kupriyanova, T.A., Welter, L., and Quigley, J.P. (2014). Tissue-infiltrating neutrophils constitute the major in vivo source of angiogenesis-inducing MMP-9 in the tumor microenvironment. Neoplasia *16*, 771–788.

Egeblad, M., Nakasone, E.S., and Werb, Z. (2010). Tumors as organs: Complex tissues that interface with the entire organism. Dev. Cell *18*, 884–901.

Fibla, J.J., Cassivi, S.D., Decker, P.A., Allen, M.S., Darling, G.E., Landreneau, R.J., McKenna, R.J., and Putnam, J.B.; ACOSOG Z0030 Study Group (2013). Validation of the lung cancer staging system revisions using a large prospective clinical trial database (ACOSOG Z0030). Eur. J. Cardiothorac. Surg. *43*, 911–914.

Folkman, J. (2002). Role of angiogenesis in tumor growth and metastasis. Semin. Oncol. *29* (*6, Suppl 16*), 15–18.

Giampieri, S., Manning, C., Hooper, S., Jones, L., Hill, C.S., and Sahai, E. (2009). Localized and reversible TGFbeta signalling switches breast cancer cells from cohesive to single cell motility. Nat. Cell Biol. *11*, 1287–1296.

Gligorijevic, B., Wyckoff, J., Yamaguchi, H., Wang, Y., Roussos, E.T., and Condeelis, J. (2012). N-WASP-mediated invadopodium formation is involved in intravasation and lung metastasis of mammary tumors. J. Cell Sci. *125*, 724–734.

Hanahan, D., and Weinberg, R.A. (2011). Hallmarks of cancer: The next generation. Cell *144*, 646–674.

Harney, A.S., Arwert, E.N., Entenberg, D., Wang, Y., Guo, P., Qian, B.Z., Oktay, M.H., Pollard, J.W., Jones, J.G., and Condeelis, J.S. (2015). Real-time imaging reveals local, transient vascular permeability, and tumor cell intravasation stimulated by TIE2hi macrophage-derived VEGFA. Cancer Discov. *5*, 932–943.

Hölzel, D., Eckel, R., Emeny, R.T., and Engel, J. (2010). Distant metastases do not metastasize. Cancer Metastasis Rev. *29*, 737–750.

Hüsemann, Y., Geigl, J.B., Schubert, F., Musiani, P., Meyer, M., Burghart, E., Forni, G., Eils, R., Fehm, T., Riethmüller, G., and Klein, C.A. (2008). Systemic spread is an early step in breast cancer. Cancer Cell *13*, 58–68.

Juncker-Jensen, A., Deryugina, E.I., Rimann, I., Zajac, E., Kupriyanova, T.A., Engelholm, L.H., and Quigley, J.P. (2013). Tumor MMP-1 activates endothelial PAR1 to facilitate vascular intravasation and metastatic dissemination. Cancer Res. *73*, 4196–4211.

Kalluri, R., and Weinberg, R.A. (2009). The basics of epithelial-mesenchymal transition. J. Clin. Invest. *119*, 1420–1428.

Kedrin, D., Gligorijevic, B., Wyckoff, J., Verkhusha, V.V., Condeelis, J., Segall, J.E., and van Rheenen, J. (2008). Intravital imaging of metastatic behavior through a mammary imaging window. Nat. Methods *5*, 1019–1021.

Kim, J., Yu, W., Kovalski, K., and Ossowski, L. (1998). Requirement for specific proteases in cancer cell intravasation as revealed by a novel semiquantitative PCR-based assay. Cell *94*, 353–362.

Klein, C.A. (2009). Parallel progression of primary tumours and metastases. Nat. Rev. Cancer *9*, 302–312.

Kovacs, E., Zorn, J.A., Huang, Y., Barros, T., and Kuriyan, J. (2015). A structural perspective on the regulation of the epidermal growth factor receptor. Annu. Rev. Biochem. *84*, 739–764.

Massagué, J., and Obenauf, A.C. (2016). Metastatic colonization by circulating tumour cells. Nature *529*, 298–306.

Minder, P., Zajac, E., Quigley, J.P., and Deryugina, E.I. (2015). EGFR regulates the development and microarchitecture of intratumoral angiogenic vasculature capable of sustaining cancer cell intravasation. Neoplasia *17*, 634–649.

Partridge, J.J., Madsen, M.A., Ardi, V.C., Papagiannakopoulos, T., Kupriyanova, T.A., Quigley, J.P., and Deryugina, E.I. (2007). Functional analysis of matrix metalloproteinases and tissue inhibitors of metalloproteinases differentially expressed by variants of human HT-1080 fibrosarcoma exhibiting high and low levels of intravasation and metastasis. J. Biol. Chem. *282*, 35964–35977.

Podsypanina, K., Du, Y.C., Jechlinger, M., Beverly, L.J., Hambardzumyan, D., and Varmus, H. (2008). Seeding and propagation of untransformed mouse mammary cells in the lung. Science *321*, 1841–1844.

Ramirez, N.E., Zhang, Z., Madamanchi, A., Boyd, K.L., O'Rear, L.D., Nashabi, A., Li, Z., Dupont, W.D., Zijlstra, A., and Zutter, M.M. (2011). The $\alpha_2\beta_1$ integrin is

a metastasis suppressor in mouse models and human cancer. J. Clin. Invest. *121*, 226–237.

Rhim, A.D., Mirek, E.T., Aiello, N.M., Maitra, A., Bailey, J.M., McAllister, F., Reichert, M., Beatty, G.L., Rustgi, A.K., Vonderheide, R.H., et al. (2012). EMT and dissemination precede pancreatic tumor formation. Cell *148*, 349–361.

Riedl, C.C., Slobod, E., Jochelson, M., Morrow, M., Goldman, D.A., Gonen, M., Weber, W.A., and Ulaner, G.A. (2014). Retrospective analysis of 18F-FDG PET/CT for staging asymptomatic breast cancer patients younger than 40 years. J. Nucl. Med. *55*, 1578–1583.

Suh, D.H., Kim, T.H., Kim, J.W., Kim, S.Y., Kim, H.S., Lee, T.S., Chung, H.H., Kim, Y.B., Park, N.H., and Song, Y.S. (2013). Improvements to the FIGO staging for ovarian cancer: Reconsideration of lymphatic spread and intraoperative tumor rupture. J. Gynecol. Oncol. *24*, 352–358.

Turajlic, S., and Swanton, C. (2016). Metastasis as an evolutionary process. Science *352*, 169–175.

Weinberg, R.A. (2013). The Biology of Cancer (Taylor & Francis Group).

Wyckoff, J.B., Wang, Y., Lin, E.Y., Li, J.F., Goswami, S., Stanley, E.R., Segall, J.E., Pollard, J.W., and Condeelis, J. (2007). Direct visualization of macrophage-assisted tumor cell intravasation in mammary tumors. Cancer Res. *67*, 2649–2656.

Xue, C., Wyckoff, J., Liang, F., Sidani, M., Violini, S., Tsai, K.L., Zhang, Z.Y., Sahai, E., Condeelis, J., and Segall, J.E. (2006). Epidermal growth factor receptor overexpression results in increased tumor cell motility in vivo coordinately with enhanced intravasation and metastasis. Cancer Res. *66*, 192–197.

Ye, X., and Weinberg, R.A. (2015). Epithelial-mesenchymal plasticity: A central regulator of cancer progression. Trends Cell Biol. *25*, 675–686.

Yoshida, Y., Murayama, T., Sato, Y., Suzuki, Y., Saito, H., and Tanaka, N. (2013). Validation of 7th TNM staging system for lung cancer, based on surgical outcomes. Asian Cardiovasc. Thorac. Ann. *21*, 693–699.